Electronic Supplementary Material (ESI) for Journal of Materials Chemistry A.

Supportive Information for

Pushing Efficiency Limits for Semitransparent Perovskite Solar Cells

César Omar Ramírez Quiroz[† a], *Ievgen Levchuk*[a], *Carina Bronnbauer*[a,b], *Michael Salvador*[a,c], *Karen Forberich*[a], *Thomas Heumüller*[a], *Yi Hou*[a,c], *Peter Schweizer*[d], *Erdmann Spiecker*[d], *Christoph J. Brabec*[a,e]

[a]Institute of Materials for Electronics and Energy Technology (I-MEET), Department of Materials Science and Engineering, Friedrich-Alexander University Erlangen-Nuremberg, Martensstrasse 7, 91058 Erlangen, Germany.

[b]Erlangen Graduate School in Advanced Optical Technologies (SAOT), Paul-Gordan-Str. 6, 91052 Erlangen, Germany.

[c]Instituto de Telecomunicações, Instituto Superior Técnico, Av. Rovisco Pais, P-1049-001 Lisboa, Portugal.

[d]Center for Nanoanalysis and Electron Microscopy (CENEM), Department Werkstoffwissenschaften, Friedrich-Alexander University Erlangen-Nuremberg, Cauerstraße 6, 91058 Erlangen, Germany.

[e]Bavarian Center for Applied Energy Research (ZAE Bayern), Am Weichselgarten 7, 91058 Erlangen, Germany.

KEYWORDS. Semitransparency, perovskite photovoltaics, morphology, ultra-thin perovskite layer, room-temperature.

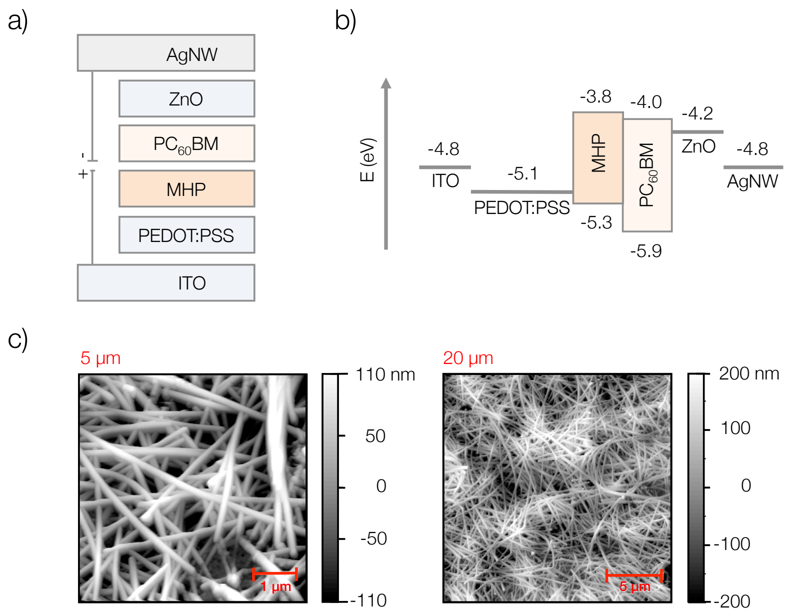

Figure S1. Schematic structure of device configuration a). Energy diagram alignment b). AFM micrograph of thick AgNW layer, showing representative AgNW morphology.

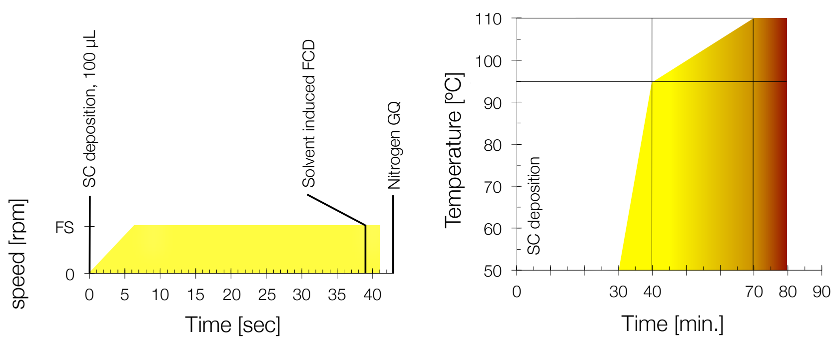

Figure S2. Schematic representation of the deposition process with FCD-GQ (left hand side) and the multi-step slow annealing profile (right hand side). The film is spin coated at the final speed (FS) with an acceleration time of 6 seconds and a spinning time of 35 seconds. At the second 39 the film its washed with 300 µL of Chlorobenzene and then dried with a moderately strong flux of nitrogen during 10 seconds with the gun pointed 90 º from the surface normal at a distance of 5 to 10 cm.

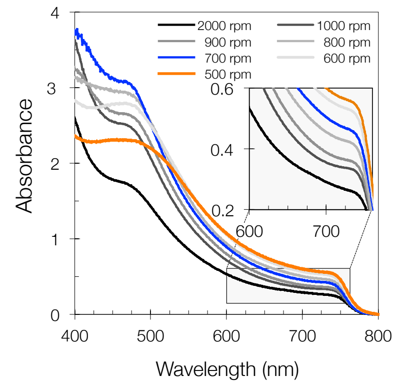

Figure S3. Absorbance spectra of bare perovskite active layers deposited at different speeds with the FCD-GQ method. Films casted at 600 and 500 rpm show a downtrend in the band of wavelengths below 500 nm.

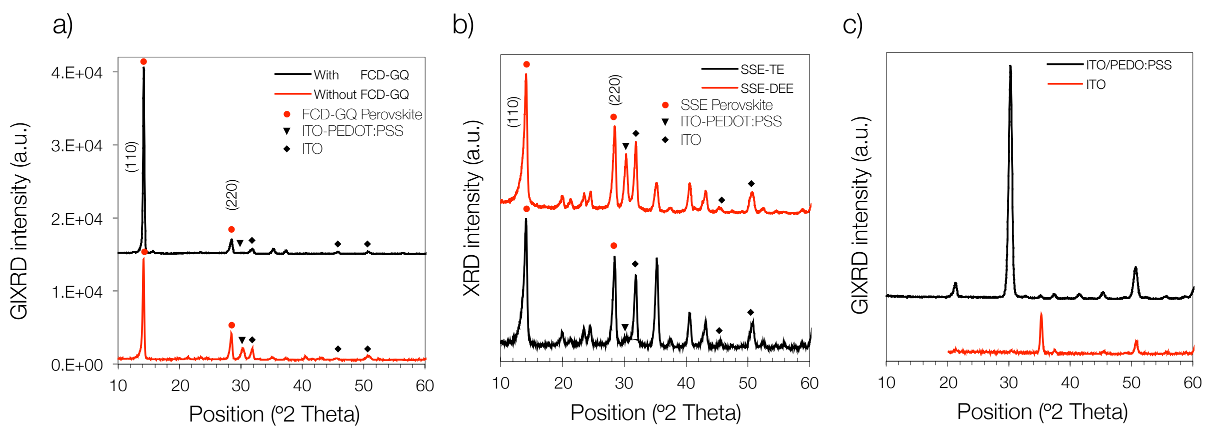

Figure S4. a) Diffractions peak intensities corresponding to perovskite films fabricated with and without FCD-GQ treatment, resulting in a difference in the (110):(220) intensity peak ratio. b) GIXRD patterns for bare films fabricated with the SSE method in ambient conditions (25ºC, 45% RH) using toluene and diethyl ether as antisolvents. c) Full GIXRD patterns of PEDOT:PSS film and ITO layer.

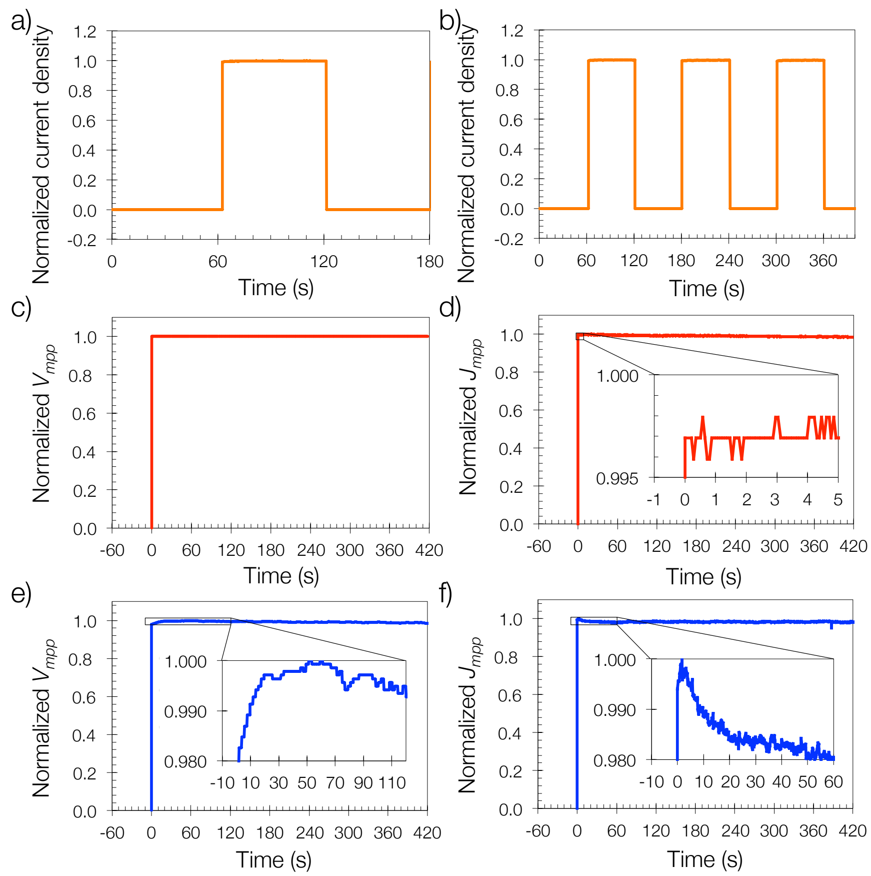

Figure S5. Photocurrent responses over time of semitransparent devices. All values are normalized by J-V characterization. All measurements were taken under illumination with a solar simulator emitting an AM 1.5G spectrum at 0.1 Wcm^2. a) Current density response for one on and off cycle. b) Consecutive on-off cycles. Normalized applied voltage corresponding to the maximum power point (V_{mpp}) of J-V characterization, c) and e). Normalized, measured current density at maximum power point (J_{mpp}), d) and f). In e) V_{mpp} is interpolated from J-V measured every second and applied to the cell, f) is measured by applying the updated V_{mpp}. d) is measured under initial V_{mpp} conditions.

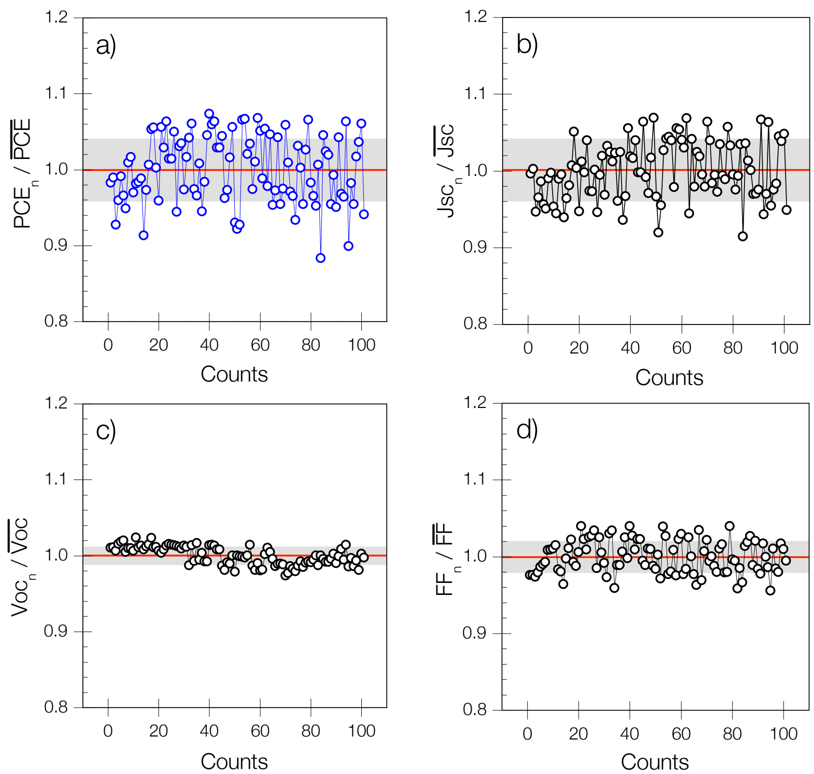

Figure S6. Variation of metrics over 100 devices, where the gray boxes represent the error within 2 standard deviations, and the red line is the average. All values are normalized by the average value. *J-V* characterization was performed under LED illumination under nitrogen atmosphere.

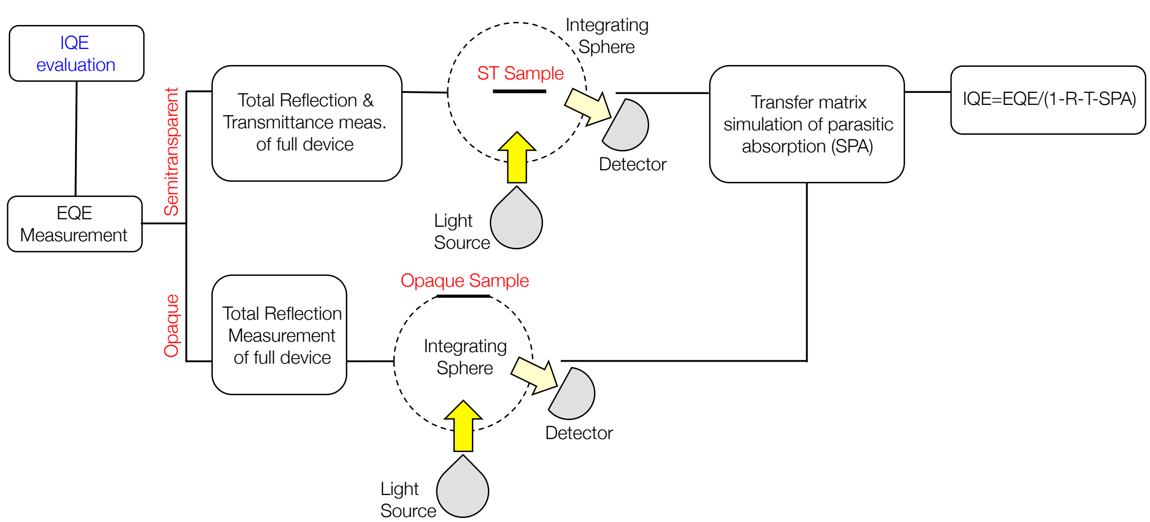

Figure S7. Flowchart for the *IQE* evaluation, on opaque and semitransparent devices, accounting for all cavity interference and parasitic absorption effect.

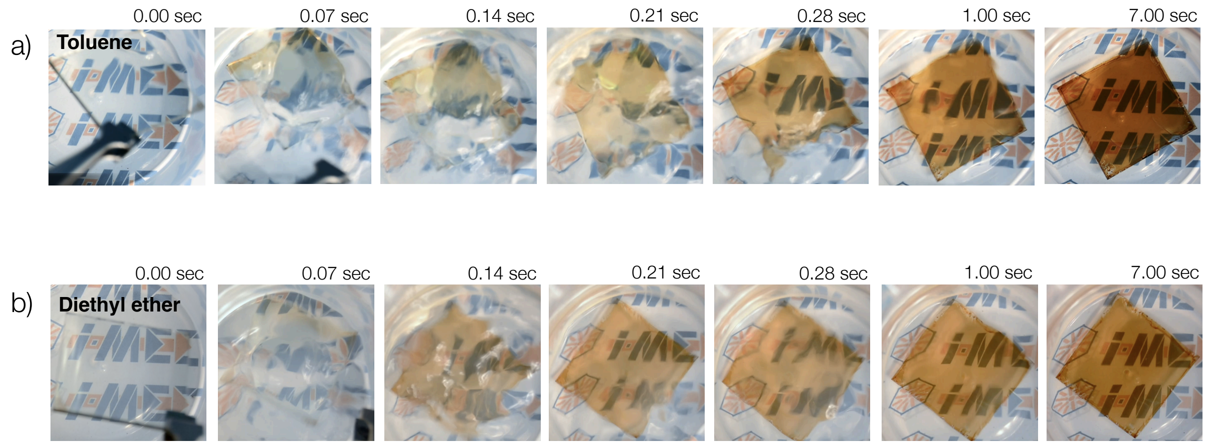

Figure S8. Time lapse sequence for solvent-solvent extraction fast crystallization of a thin perovskite layer over the structure glass/ITO/PEDOT:PSS. Process was recorded in ambient conditions (25ºC and 45 %RH). Anti-solvents were toluene and diethyl ether for a) and b), respectively. See also complementary video.

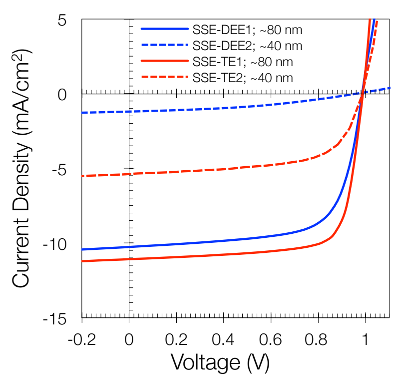

Figure S9. *J-V* characterization for devices made with the DEE method. Comparison between toluene and diethyl ether extraction solvents, showing how toluene performs better for in highly transparent devices with thin perovskite films.

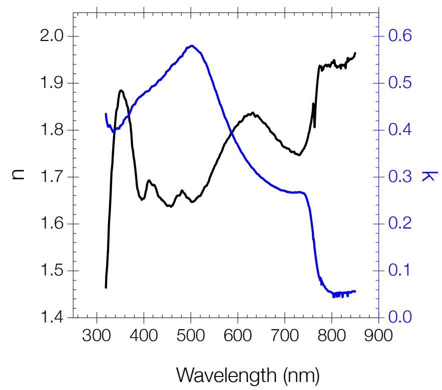

Figure S10. Optical constants *n* and *k* obtained by measuring total transmission and total reflection spectra of a peroskite film assisted with FCD-GQ with a thickness of 280 nm. Optical constants were modeled with software NIKA (commercially available in: http://lpvo.fe.uni-lj.si/en/software/nika/).

Table S1. Metrics summary for opaque devices using the FCD-GQ method. Thickness and grain size information.

ID	*Grain Size (μm)*[1]	*Thickness (nm)*[1]	*EQE Mea. (mA/cm²)*[1]	*PCE (%)*[1,2]
FCD-OP1	~	72 (70±18)	14.59 (14.54±0.04)	10.12 (10.10±0.02)
FCD-OP2	~	102 (100±18)	15.61 (15.38±0.16)	10.71 (10.47±0.17)
FCD-OP3	1.41 (0.86±0.24)[3]	158 (129±18)	17.54 (17.43±0.08)	12.20 (12.04 ±0.14)
FCD-OP4	2.23 (0.95±0.41)	259 (238±16)	20.36 (20.32±0.04)	14.97 (14.69±0.24)
FCD-OP5	2.47 (1.65±0.44)	295 (272±17)	20.38 (20.22±0.22)	14.51 (14.38±0.10)
FCD-OP6	4.13 (1.92±0.73)	310 (298±18)	20.91 (20.89±0.01)	14.43 (14.31±0.14)
FCD-OP7	6.49 (3.41±1.09)	366 (339±16)	21.93 (21.56±0.32)	15.99 (15.75±0.24)

[1] Grain size statistics were taken over 100 measurements, Thickness values 10 measurements, and *PCE* and *EQE* values were taken from 12 working devices.

[2] *PCE* values are calculated using short circuit photocurrent extracted from EQE measurement.

[3] The display of the results is as follows: maximum value (arithmetic mean ± standard deviation).

Table S2. Metrics extracted from *J-V* characterization of opaque devices using the FCD-GQ method under solar simulator.

ID	*PCE* (%)[1]	*FF* (%)	*Jsc* (mA/cm^2)	*Voc* (V)
FCD-OP1	11.45 (10.10±0.02)[2]	75.81 (74.41±1.93)	15.91 (14.78±0.94)	0.96 (0.96 ±0.00)
FCD-OP2	11.23 (11.03±0.17)	73.63 (73.00±0.43)	16.27 (15.38±0.37)	0.96 (0.96 ±0.00)
FCD-OP3	12.20 (12.04±0.15)	74.55 (73.03±1.30)	18.79 (18.49±0.30)	0.94 (0.94 ±0.00)
FCD-OP4	14.97 (14.69±0.24)	78.62 (77.21±0.76)	20.43 (19.87±0.70)	0.95 (0.95 ±0.01)
FCD-OP5	14.38 (14.51±0.10)	75.14 (73.97±0.88)	20.20 (20.18±0.87)	0.96 (0.95 ±0.01)
FCD-OP6	14.43 (14.31±0.14)	71.98 (71.70±0.25)	21.30 (20.26±1.93)	0.96 (0.94 ±0.03)
FCD-OP7	15.99 (15.75±0.24)	76.06 (74.13±1.37)	22.05 (21.93±2.95)	0.99 (0.97 ±0.03)

[1] *PCE* values are calculated using short circuit photocurrent extracted from *J-V* characterization.

[2] The display of the results is as follows: maximum value (arithmetic mean ± standard deviation) over 12 devices.

Table S3. Metrics summary of semitransparent devices using the FCD-GQ method..

ID	*Thickness (nm)*	*EQE Mea. (mA/cm^2)*	*PCE (%)*[1]	AVT^a	AVT^b	$T^a_{550\ nm}$	$T^b_{550\ nm}$
FCD-ST1	72 (70±14)	11.55 (11.40±0.10)	7.81 (7.68±0.10)	42	37	27	24
FCD-ST2	102 (100±17)	14.23 (13.99±0.26)	9.55 (9.47±0.06)	33	29	20	17
FCD-ST3	158 (129±18)	17.32 (17.01±0.54)	10.81 (10.58±0.17)	28	23	12	9
FCD-ST4	366 (339±16)	19.10 (18.90±0.14)	12.95 (12.78±0.17)	18	14	4	1

[1] *PCE* values are calculated using short circuit photocurrent extracted from *J-V* characterization.

AVT^a is the % average total transmittance measured in device excluding the electrode. AVT^b is for full device. Both measured in the range of wavelength 400-800 nm. *T* is the % transmittance at 550 nm. The super index '*a'* refers to devices excluding the electrode and '*b'* is for full cell.

Table S4. Metrics extracted from *J-V* characterization of semitransparent devices using the FCD-GQ method under solar simulator.

ID	*PCE* (%)[1]	*FF* (%)	*Jsc* (mA/cm^2)	*Voc* (V)
FCD-ST1	7.95 (7.47±0.02)[2]	72.23 (70.47±1.77)	11.83 (11.22±0.59)	0.97 (0.96 ±0.01)
FCD-ST2	10.15 (9.60±0.17)	72.07 (69.47±2.30)	14.91 (14.27±0.43)	0.98 (0.97 ±0.01)
FCD-ST3	11.41 (10.88±0.32)	69.38 (65.71±2.36)	19.97 (17.01±1.26)	0.97 (0.97 ±0.01)
FCD-ST4	12.95 (12.78±0.17)	70.86 (69.96±0.65)	21.44 (19.19±1.44)	0.97 (0.96 ±0.01)

[1] *PCE* values are calculated using short circuit photocurrent extracted from *J-V* characterization.

[2] The display of the results is as follows: maximum value (arithmetic mean ± standard deviation) over 12 devices.

Table S5. Metrics summary of semitransparent devices using the SSE method.

ID	*Thickness (nm)*	*EQE Mea. (mA/cm^2)*	AVT^{a}	AVT^{b}	$T^{a}_{550\,nm}$	$T^{b}_{550\,nm}$
SSE-TE1	84±19	9.54 (9.44±0.10)	33	28	18	15
SSE-TE2	40±24	4.37 (4.30±0.05)	50	46	45	42

AVT^{a} is the % average total transmittance measured in device excluding the electrode. AVT^{b} is for full device. Both measured in the range of wavelength 400-800 nm. *T* is the % transmittance at 550 nm. The super index '*a*' refers to devices excluding the electrode and '*b*' is for full cell.

Table S6. Metrics extracted from *J-V* characterization of semitransparent devices using the SSE method under solar simulator.

ID	*PCE* (%)[1]	*FF* (%)	*Jsc* (mA/cm^2)	*Voc* (V)
SSE-TE1	**8.12** (7.70±0.38)[2]	71.77 (70.00±1.55)	11.22 (11.22±0.27)	1.03 (1.03±0.01)
SSE-TE2	**3.55** (3.07±0.37)	65.55 (63.50±1.69)	5.40 (4.79±1.44)	1.03 (1.01 ±0.01)

[1] *PCE* values are calculated using short circuit photocurrent extracted from *J-V* characterization.

[2] The display of the results is as follows: maximum value (arithmetic mean ± standard deviation) over 12 devices.

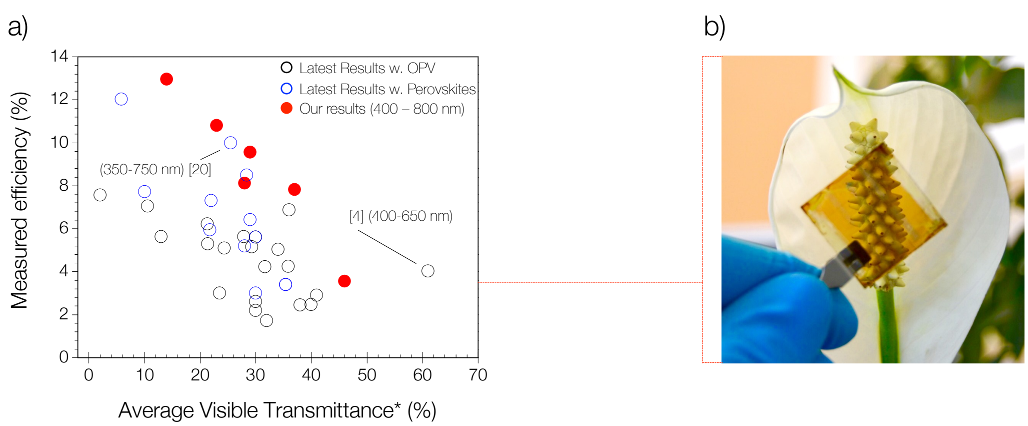

Figure S11. a) Comparison between our results and recent progress in OPV[1–13] (solid black circles) and the latest semitransparent perovskite reports[14–20] (solid blue circles) in terms of average visible transmittance. The reported average transmittance plotted varies in range being 400 nm to 800 nm the broadest. b) Digital image of a full cell fabricated with the SSE-TE approach.

REFERENCES

(1) Forberich, K.; Guo, F.; Bronnbauer, C.; Brabec, C. J. Efficiency Limits and Color of Semitransparent Organic Solar Cells for Application in Building-Integrated Photovoltaics. *Energy Technol.* **2015**, *3*, 1–9.

(2) Beiley, Z. M.; Christoforo, M. G.; Gratia, P.; Bowring, A. R.; Eberspacher, P.; Margulis, G. Y.; Cabanetos, C.; Beaujuge, P. M.; Salleo, A.; McGehee, M. D. Semi-Transparent Polymer Solar Cells with Excellent Sub-Bandgap Transmission for Third Generation Photovoltaics. *Adv. Mater.* **2013**, *25* (48), 7020–7026.

(3) Da Silva, W. J.; Kim, H. P.; Rashid bin Mohd Yusoff, A.; Jang, J. Transparent Flexible Organic Solar Cells with 6.87% Efficiency Manufactured by an All-Solution Process. *Nanoscale* **2013**, *5* (19), 9324–9329.

(4) Chen, C. C.; Dou, L.; Zhu, R.; Chung, C. H.; Song, T. Bin; Zheng, Y. B.; Hawks, S.; Li, G.; Weiss, P. S.; Yang, Y. Visibly Transparent Polymer Solar Cells Produced by Solution Processing. *ACS Nano* **2012**, *6* (8), 7185–7190.

(5) Kim, H. P.; Lee, H. J.; Mohd Yusoff, A. R. Bin; Jang, J. Semi-Transparent Organic Inverted Photovoltaic Cells with Solution Processed Top Electrode. *Sol. Energy Mater. Sol. Cells* **2013**, *108*, 38–43.

(6) Guo, F.; Zhu, X.; Forberich, K.; Krantz, J.; Stubhan, T.; Salinas, M.; Halik, M.; Spallek, S.; Butz, B.; Spiecker, E.; et al. ITO-Free and Fully Solution-Processed Semitransparent Organic Solar Cells with High Fill Factors. *Adv. Energy Mater.* **2013**, *3* (8), 1062–1067.

(7) Pastorelli, F.; Romero-Gomez, P.; Betancur, R.; Martinez-Otero, A.; Mantilla-Perez, P.; Bonod, N.; Martorell, J. Enhanced Light Harvesting in Semitransparent Organic Solar Cells Using an Optical Metal Cavity Configuration. *Adv. Energy Mater.* **2014**, *5*, 1400614.

(8) Chen, K.-S.; Salinas, J.-F.; Yip, H.-L.; Huo, L.; Hou, J.; Jen, A. K.-Y. Semi-Transparent Polymer Solar Cells with 6% PCE, 25% Average Visible Transmittance and a Color Rendering Index close to 100 for Power Generating Window Applications. *Energy Environ. Sci.* **2012**, *5* (11), 9551.

(9) Ameri, T.; Dennler, G.; Waldauf, C.; Azimi, H.; Seemann, A.; Forberich, K.; Hauch, J.; Scharber, M.; Hingerl, K.; Brabec, C. J. Fabrication, Optical Modeling, and Color Characterization of Semitransparent Bulk-Heterojunction Organic Solar Cells in an Inverted Structure. *Adv. Funct. Mater.* **2010**, *20* (10), 1592–1598.

(10) Yu, W.; Shen, L.; Shen, P.; Meng, F.; Long, Y.; Wang, Y.; Lv, T.; Ruan, S.; Chen, G. Simultaneous Improvement in Efficiency and Transmittance of Low Bandgap Semitransparent Polymer Solar Cells with One-Dimensional Photonic Crystals. *Sol. Energy Mater. Sol. Cells* **2013**, *117*, 198–202.

(11) Guo, F.; Kubis, P.; Stubhan, T.; Li, N.; Baran, D.; Przybilla, T.; Spiecker, E.; Forberich, K.; Brabec, C. J. Fully Solution-Processing Route toward Highly Transparent Polymer Solar Cells. *ACS Appl. Mater. Interfaces* **2014**, *6*, 18251−18257.

(12) Betancur, R.; Romero-Gomez, P.; Martinez-Otero, A.; Elias, X.; Maymó, M.; Martorell, J. Transparent Polymer Solar Cells Employing a Layered Light-Trapping Architecture. *Nat. Photonics* **2013**, *7* (October), 995–1000.

(13) Yu, W.; Shen, L.; Shen, P.; Long, Y.; Sun, H.; Chen, W.; Ruan, S. Semitransparent Polymer Solar Cells with 5% Power Conversion Efficiency Using Photonic Crystal Reflector. *ACS Appl. Mater. Interfaces* **2014**, *6* (1), 599–605.

(14) Eperon, G. E.; Burlakov, V. M.; Goriely, A.; Snaith, H. J. Neutral Color Semitransparent Microstructured Perovskite Solar Cells. *ACS Nano* **2014**, *8* (1), 591–598.

(15) Eperon, G. E.; Bryant, D.; Troughton, J.; Stranks, S. D.; Johnston, M. B.; Watson, T.; Worsley, D. A.; Snaith, H. J. Efficient, Semitransparent Neutral-Colored Solar Cells Based on Microstructured Formamidinium Lead Trihalide Perovskite. *J. Phys. Chem. Lett.* **2015**, *6*, 129−138.

(16) Roldan, C.; Malinkiewicz, O.; Betancur, R.; Longo, G.; Momblona, C.; Jaramillo, F.; Camacho, L.; Bolink, H. J. High Efficiency Single-Junction Semitransparent Perovskite Solar Cells. *Energy Environ. Sci.* **2014**, *7*, 2968–2973.

(17) Li, Z.; Kulkarni, S. a; Boix, P. P.; Shi, E.; Cao, A.; Fu, K.; Batabyal, S. K. Laminated Carbon Nanotube Networks for Metal Electrode-Free. *ACS Nano* **2014**, *8* (7), 6797–6804.

(18) Guo, F.; Azimi, H.; Hou, Y.; Przybilla, T.; Hu, M.; Bronnbauer, C.; Langner, S.; Spiecker, E.; Forberich, K.; Brabec, C. J. High-Performance Semitransparent Perovskite Solar Cells with Solution-Processed Silver Nanowires as Top Electrodes. *Nanoscale* **2014**, *7*, 1642–1649.

(19) You, P.; Liu, Z.; Tai, Q.; Liu, S.; Yan, F. Efficient Semitransparent Perovskite Solar Cells with Graphene Electrodes. *Adv. Mater.* **2015**, *27*, 3632–3638.

(20) Chih-Yu Chang; Kuan-Ting Lee; Wen-Kuan Huang; Hao-Yi Siao; Yu-Chia Chang. High-Performance, Air-Stable, Low-Temperature Processed Semitransparent Perovskite Solar Cells Enabled by Atomic Layer Deposition. *Chem. Mater.* **2015**, *27* (14), 5122–5130.